Pergamon

Solid State Communications, Vol. 107, No. 11, pp. 597–606, 1998

0038–1098/98 $ - see front matter

PII: S0038–1098(98)00210-5

THE FUTURE OF THE FULLERENES

Richard E. Smalley[a,*] and Boris I. Yakobson[b]

[a]Center for Nanoscale Science and Technology, Rice University, P.O. Box 1892, MS 100, Houston, TX 77251, U.S.A.

[b]Department of Materials Science and Engineering, Rensselaer Polytechnic Institute, Troy, NY 12180, U.S.A.

As the fullerene studies progress, two trends become more visible: the incorporation of the smaller cages of C_{60} type into organic chemistry and the increasing interest in the elongated fullerene species, carbon nanotubes. The latter turn out to be of interest for structural materials and for the sub-micro-electronics application. The mechanical strength of these molecular fibers combines with electronic properties, that are uniquely tunable by the molecular symmetry of nanotubes. We outline the basic features of fullerene nanotubes and the more recent findings in their mechanical and electrical properties.

1. FROM BALLS TO CONES TO TUBES

The family of fullerenes – generally hollow molecules made of carbon – emerged into real world in 1985 with the discovery of the smallest member, the buckyball C_{60} [1, 2]. The decade which followed has led to a formation of comprehensive knowledge as presented in excellent recent monographs [3, 4] and several review articles. Here we briefly outline the latest findings and facts, preceding them by introduction of some basic properties and concentrating mostly on nanotubes. A fullerene, by definition, is a closed convex cage molecule containing only hexagonal and pentagonal faces. This definition intentionally leaves out possible heptagons, which are therefore treated as ''defects'' and are responsible for concave parts. As any simple polyhedron, a fullerene cage or a nanotube satisfies Descartes-Euler's theorem, relating the number of *v*ertices (carbon atoms), *e*dges (covalent bonds) and *f*aces: $v - e + f = 2$. If the number of pentagons is p and the other $(f - p)$ faces are all hexagonal, then the doubled number of edges (each edge belongs to the *two* faces) is $5p + 6(f - p)$, which also equals the tripled number of vertices (each trivalent carbon is shared by *three* adjacent faces). A simple accounting then yields $p = 12$. In a broader sense, fullerenes also include largely elongated cages (nano-*tubes* [5]), *multishell* tubes and ''*onions*'' and *cones* [6, 7]. In the more complex geometries, local curvature often requires the presence of a heptagon and therefore (to satisfy Euler's rule) a greater number $p > 12$ of pentagons as well. Recently identified series of cones [7] allows to bridge the possible topological structures, from the C_{60} and other small cages to unlimited cylinders-nanotubes. Although the details of the nucleation and growth mechanism remain largely hypothetical, the cones present solid evidence of the role played by initial number of pentagons-disclinations, imbedded at the foundation of the growing structure. Further growth is mainly epitaxial extension, terminated sooner or later by other causes, yet to be understood. The existence of the exactly seven shapes, diverging at different angle from the seed-nucleation point, clearly corresponds to a different number of pentagons in the cap-apex, Fig. 1(a)–(e). Insertion of a pentagon in the hexagonal graphene sheet reduces the plate angle by $p/3$, so that the presence of p pentagons corresponds to the cone angle,

$$\theta = 2 \arcsin(1 - p/6). \tag{1}$$

This allows for the possibility of disks ($p = 0$ and $\theta = 180°$), five cones ($p = 1, \ldots, 5$ and $\theta = 113°$, 84°, 60°, 39°, 19.2°) and tubules-cylinders ($p = 6$, $\theta = 0$). Any $p > 6$ causes immediate convergence in a closed cage ($p = 12$) and the C_{60} turns out to be the most

* Corresponding author.

frequent one, Fig. 1(f) [8]. Remarkably, the disks and all five cones have been clearly observed in experiment [7], although several years later than the closed cages and nanotubes.

In the context of solid state studies and applications, small fullerene *cages* and C_{60} in particular are usually discussed in their condensed-matter state as molecular crystals. At room temperature C_{60} crystallizes in a cubic structure and the molecules are shown (by NMR methods) to be almost freely rotating, that is all three rotational degrees are "melted". The crystalline forms of fullerenes are often called fullerites and a bulk of knowledge about them has been accumulated [3].

Cones, in contrast, are simply too large and variable in size to imagine their condensation in a regular sense. Every single cone represents actually a nano-scale structure and their properties are scarcely known or discussed.

Fullerene *nanotubes* (Fig. 2) occupy unique intermediate position between molecules and material. Their elongation (aspect ratio of $> 10^4$ is realistic) and periodic structure makes the nanotubes essentially one-dimensional crystals and allows discussion of transport properties and mechanical moduli for a single tube. Beyond that, at certain growth conditions [9] single-wall nanotubes tend to form well-organized crystalline structure in the two other (perpendicular to the axis) directions as well, aggregating in *ropes* [Fig. 2(b)]. High-resolution imaging with TEM shows triangular lattice, with almost identical in diameter (1.4 nm) nanotubes and the lattice spacing of 1.7 nm. The future of this branch of the fullerene family is of special interest for solid state physics and materials science and some of the properties are briefly discussed below.

2. MORPHOLOGY AND GROWTH

Besides the topological invariants, the nanotubes inherit an even more obvious trait from another ancestor, graphite. It is a hexagonal pattern on their walls. In a gedanken growth experiment, one can start with a piece of a one-atom-thick sheet of graphite, cut a long strip out of it and roll it up into a cylinder with no stitches left. There is a decision to make though: to choose the strip width parallel to the dense zig-zag row of bonds, perpendicular to it, or at some angle χ. The first choice results in so-called zigzag nanotube ($\chi = 0$), the second – to the armchair tubule ($\chi = 30°$). The

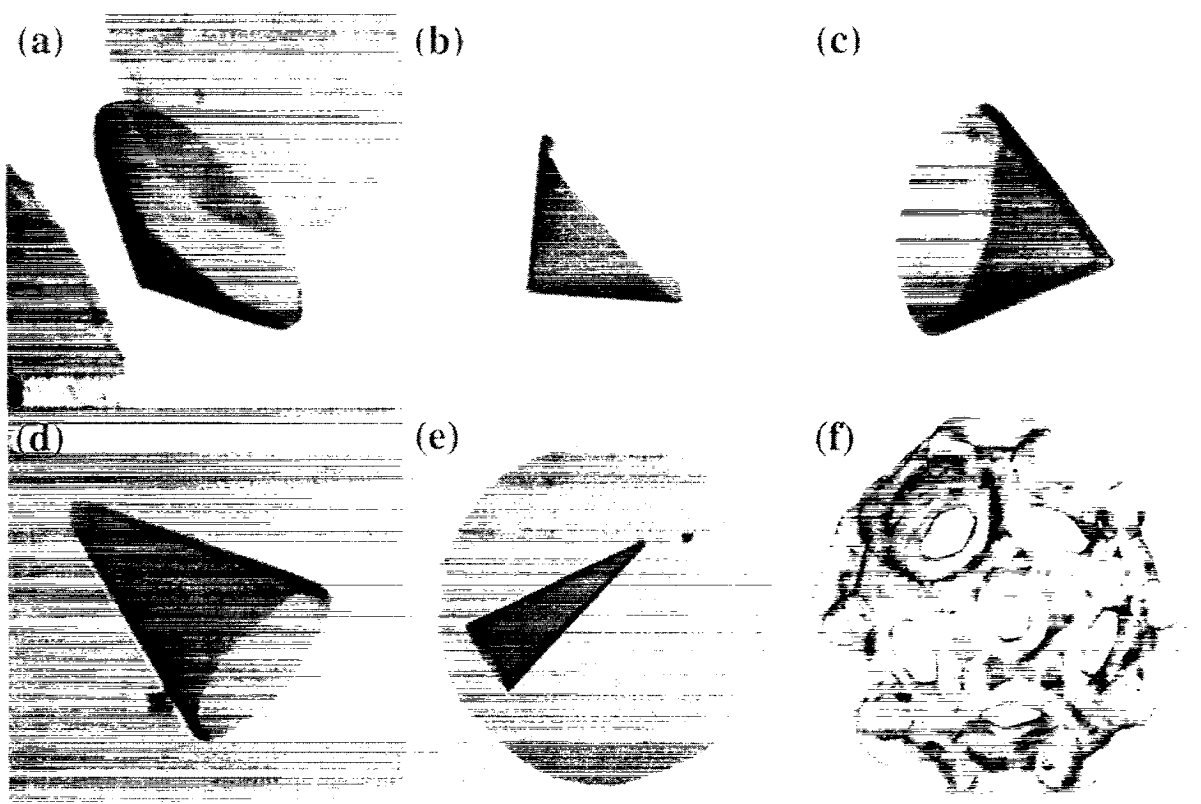

Fig. 1. Insertion of $p = 1$ to $p = 5$ pentagons in a flat graphene results in a series of five different cones [7] (a–e). (f) A greater number $p > 6$ causes closure of a fullerene cage and inevitably leads to $p = 12$ pentagons like in this C_{60} molecule (spatial electronic density image data from [8]).

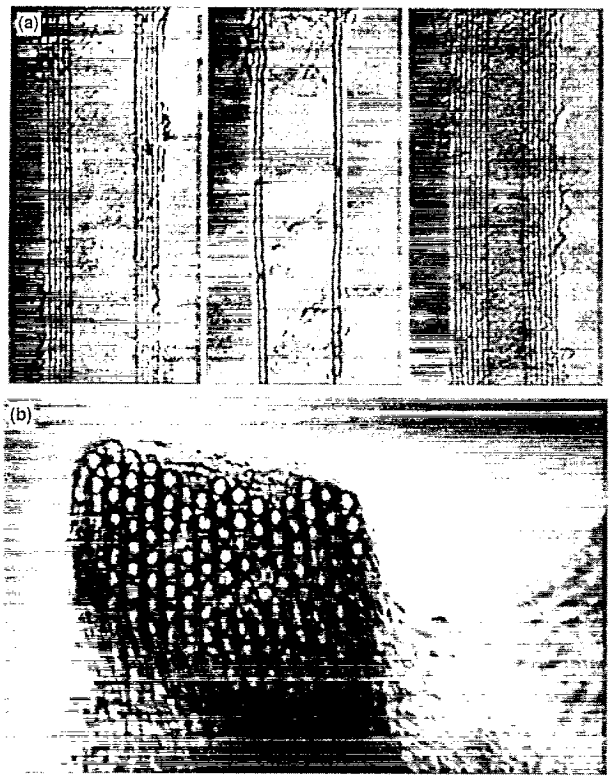

Fig. 2. (a) First high-resolution electron micrographs of CNT, 5-, 2- and 7-wall cylindrical molecules, as reported by Iijima [5]. (b) Each rope is a bundle of single-wall nanotubes of approximately 1.4 nm diameter each, arranged in a triangular lattice and is shown here as it bends through the image plane of the microscope [9].

"oriented width" is specified by a rollup vector (n,m), the number of steps along the $\mathbf{a}_1$ and $\mathbf{a}_2$ directions, Fig. 3. Its integer components uniquely define the tubule diameter d and its helicity, or a chiral angle χ. Assuming that C–C bond has its normal length of $a = 0.14$ nm,

$$d = 0.078\sqrt{n^2 + nm + m^2}\ \text{nm}, \tag{2a}$$

$$\chi = \arctan[\sqrt{3}m/(m + 2n)]. \tag{2b}$$

For example, (9,0) or (5,5) correspond to the zigzag or armchair buckytubes, roughly 0.7 nm wide. Such a seamless coherent arrangement of atoms has certain helicity and recognition of this, based on observed electron diffraction patterns, was perhaps even more important in Iijima's discovery [5] that the fact that the nanotubes are thin cylinders.

Morphology of nanotubes and their helical structure are inherently related with the growth mechanisms. The formation of these nanoscopic stalagmites in most cases requires an "open end" where the carbon atoms arriving from the gas phase could coherently land. Growth of nested multiwall nanotubes can be stabilized by the strained "lip–lip" bonding between the coaxial edges, highly fluctuating and therefore accessible for new atoms. In general, the open end can be maintained either by a high electric field, by the entropy opposing the orderly cap termination, or by the presence of a metal crystal. The latter, in a form of tiny metal (Ni or Co) cluster "scooting" around the nanotube edge [9], is apparently responsible for the high-yield growth of the tubes of uniform diameter and approximately (10,10) type. The alloy cluster anneals all unfavorable structures into hexagons, which in turn welcome the newcomers and promote the continuous growth of a straight cylindrical tower. Figure 4 illustrates the energetics of growth, the relative binding energies in nanotubes, graphite and the feedstock components.

Iijima discovered the nanotubes in the samples produced by the d.c. arc-discharge between the carbon electrodes [10] immersed in a nobel gas in an apparatus similar to that used for fullerene mass production after

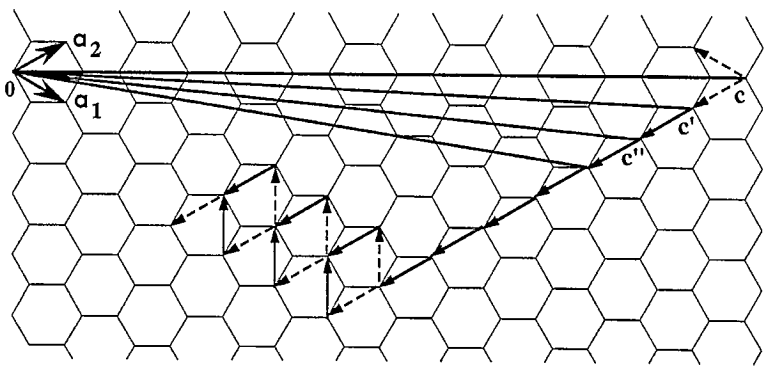

Fig. 3. With $\mathbf{a}_1$ and $\mathbf{a}_2$ as a basis in the hexagonal lattice, the CNT is specified by mapping its circumference on a vector $\mathbf{c}$. The sequence of arrows towards $\mathbf{c}'$, $\mathbf{c}''$, etc. shows a progression of the tubule helicity in the process of possible plastic necking at very high temperature (see later in the text, Section 4).

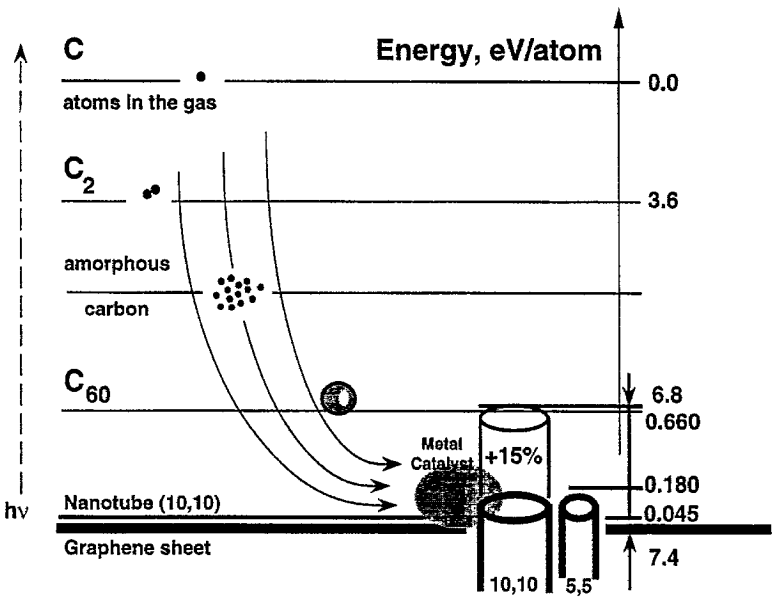

Fig. 4. "Food chain" illustrates how the metal (Ni/Co) cluster is able to eat essentially any carbon material it encounters and feed the digested carbon bits to the growing end of the nanotube. The vertical axis shows the cohesive energy per atom for the different forms of carbon consumed in nanotube growth. The energy cost for curving the graphene sheet into the cylinder of the (10,10) tube is only 0.045 eV, or 0.08 eV nm^2/d^2 for a tube of any diameter d. The elastic stretching of a tube by 15% adds approximately 0.66 eV per atom above the graphene.

Kratschmer and Huffman [2]. Although other fullerenes can be produced by different ways of vaporization of carbon, followed by condensation in tiny clusters, the presence of an electric field [11] in the arc-discharge seems to promote the growth of the long tubules. Indeed, nanotubes form only where the current flows, on the larger negative electrode. Typical rate of the cathode deposit is about a millimeter per minute, with the current and voltage in the range of 100 A and 20 V respectively, which maintains a high temperature of 2000–3000°C. Quite by chance, Ebbesen and Ajayan [12] found a way to mass produce nanotubes in high yields which made them available for studies by different techniques. Subsequently they found a way to purify them. An addition of a small amount of transition metal powder (Co, Ni, or Fe) favors a growth of so-called single-walled nanotubes, independently noticed by Bethune [13] and Ijima [14]. Metal clearly serves as a catalyst preventing the growing tubular structure from wrapping around and closing into a smaller fullerene cage. The presence of a catalyst also allows one to lower the temperature, which otherwise makes the arc just too hot a place: nanotubes coalesce and merge like the foam bubbles in a glass of beer. Condensation of laser-vaporized carbon/catalyst mixture at a lower temperature (1200°C in an oven-heated quartz tube) allowed to produce single-walled nanotubes in $> 70\%$ yield [9]. Moreover, these CNT's self-organize into bundles-ropes [Fig. 2(b)] and are more than tenth of a millimeter long.

3. ELECTRONICS

From a chemist viewpoint, the electronic structure of fullerenes and graphite relates to aromaticity. Tracing the evolution of energy levels through a series of aromatic molecules (those made of planar hexagons and hydrogen-terminated at the edge) goes back to Coulson. The smallest, benzene, is effectively a metallic ring where the six π-electrons really are free to be completely itinerant around the ring and in fact it is the lowering of the "confinement energy" for these particles in a toroidal box that is the basis of aromatic stabilization. Aromaticity is the answer to the question of how one makes electrons itinerant without simultaneously easy to remove in oxidation reactions. This remains true in naphthalene, anthracene and larger polycyclic aromatic ring systems, all the way up to a *flat* graphene sheet. As the number of atoms approaches 10^2, the density of states around the bonding–anti-bonding gap is almost the same as in an infinite graphene sheet. The same itinerant π-electrons make the fullerenes and nanotubes aromatic. Are nanotubes metallic or semiconducting? Interestingly, this question was addressed before the first real tubules have been reported and the answer was "both" [15–17].

Quantitative analysis for the tubes begins from a graphene sheet, since any tube can be visualized as a conformal mapping of a honeycomb lattice onto a curved

cylindrical surface. In graphite, the π-electrons really are completely itinerant, but the hexagonal symmetry for the flat sheet causes the band structure to be that of a zero-gap semiconductor. The simplest tight-binding model (with one parameter, the nearest neighbor overlap element γ_0) shows that the conduction and valence bands only touch each other at the end-corners K (and K') of the standard hexagonal Brillouin zone and the Fermi surface is collapsed to a point. In planar graphite there is no band gap between the empty and full states, but there are only very tiny number of electrons capable to move along the graphene sheets. Graphite therefore has the weak conductivity of a semimetal. A recently suggested treatment [18] of tube electronics is based on an expansion of the graphene π-electron Hamiltonian in the vicinity of K-corners in a form of massless Dirac Hamiltonian, $H_{\text{eff}} \sim \hat{\sigma} \cdot \mathbf{k}$, where $\hat{\sigma}$ are the Pauli matrices and $\mathbf{k}$ is the two-dimensional momentum. The tubular shape adds two effects: it imposes the Born–Karman periodic conditions around the tube waist and the element γ_0 variations due to the bond length and the misorientation of the π orbitals. This leads to the two additive contributions in the H_{eff}: the first, $\sim 2\gamma_0 a/d$, is inversely proportional to the diameter and vanishes for the tubes with $m-n$ multiple of 3; the second, $\sim 1/d^2$ is caused by the curvature [18, 19] and vanishes strictly by symmetry for $m-n=0$. The results of this model correspond well to the detailed calculations of the band gaps using atomic orbitals in the tight-binding method. There are thus three kinds of nanotubes: with nonzero primary gap $\sim 1/d$, others with zero primary gap but nonvanishing curvature-induced gap $\sim 1/d^2$ and finally the armchair tubes (n,n) with zero gap. The one-dimensional density of states (DOS) based on zone folding (no curvature effects included in γ_0) is shown in Fig. 5 for two different tubes [20]. Further, the authors of [18] conclude that the tube elastic twist, inducing a non-zero fluctuation of the "mass" term in the Hamiltonian, can be a strong scatterer for conducting π-electrons and is largely responsible for the temperature dependence of the resistivity.

In principle, any 1-dimensional metal is prone to the Peierls instability, when translational symmetry breaks and a finite band gap emerges. However, the analysis shows that the exceptional stiffness of the tube combined with the not too high carrier density at the Fermi level, makes nanotubes stable to Peierls distortion well below room temperature (see Mintmire and White, Chap. 6 in [4]). Bond-length alternations, like in polyacetylene $\cdots \div \mathrm{CH} \div \mathrm{CH} \div \mathrm{CH} \div \mathrm{CH} \div \cdots \rightarrow \cdots$ $-\mathrm{CH}=\mathrm{CH}-\mathrm{CH}=\mathrm{CH}-\cdots$, do not occur and the armchair tube remains metallic. Overall, the result of the analysis is that wrapping a graphene in an armchair tubule makes a truly metallic molecular wire that is chemically stable

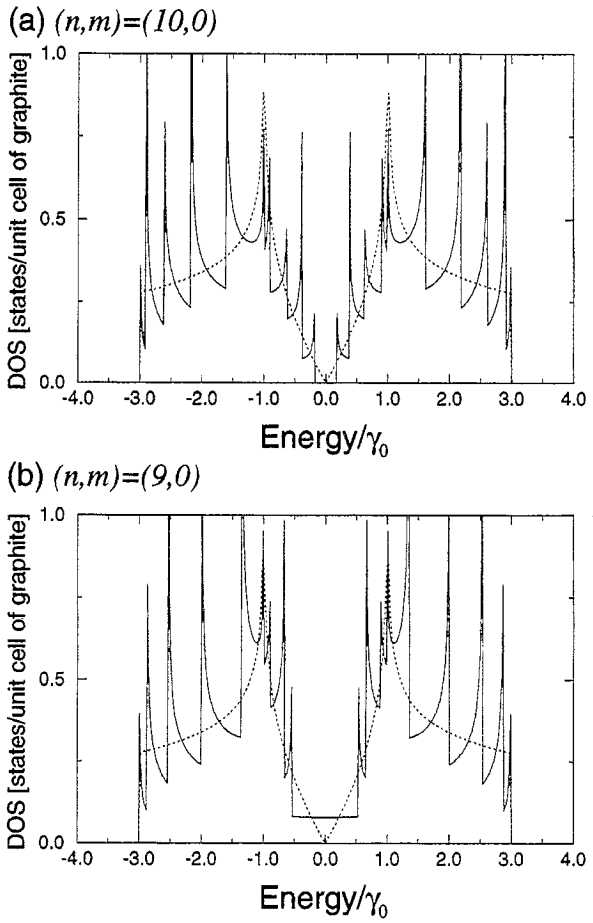

Fig. 5. A one-dimensional electronic density of states based on zone-folding of two-dimensional graphene, for two different tubes [20]: (a) the semiconducting (10,0) tube, (b) the metallic (9,0) tubule. Dashed curves show the density of states for graphene.

for reasons of aromaticity. Furthermore, doping with metals allows to increase the conducting properties.

Actual experimental attachment of contacts to a nanotube is challenging. Reports on connecting devices from the macroworld to the "molecular wires" – nanotubes came with gradual progress in probe arrangement. Variations of resistivity with temperature and magnetoresistance measurements were used to reveal the nature of conductance [21–25]. The latest reports show (direct low-temperature STM imaging [26, 27]) that the single-wall tubes have different helicity and the band gap values correlate well with this symmetry, in excellent agreement with the theoretical predictions [28]. Overall, both metallic and non-metallic CNT were found, illustrating the profound sensitivity of the electrical properties on the geometry of specific tube. The fact that metallic conductivity of the fullerene tubes is caused by their specific symmetry, makes it potentially vulnerable to all kinds of external forces. For instance,

the inter-tubule interactions in a triangular lattice of nano-ropes [made mostly of (10,10) type tubes] lowers the symmetry and results in a small gap [29]. As demonstrated experimentally, strong interaction between the tubes [30] or with the substrate [31], can flatten the cylinder and therefore also changes its symmetry and the band structure.

While the electrical conductance of CNT is an important emulation of the macro-world materials, their small size and perfect structure make them *quantum* wires. They behave like waveguides for electrons, permitting only a few propagating modes – a property more common in fiber communication optics. Instead of changing smoothly with the thickness of CNT or applied voltages, the currents through CNT go stepwise, revealing the "grainy" nature of the quantum wires. Reliable evidence of quantum-wire properties continues to accumulate [23, 25, 32]. It was first noticed in bundles of tubes, where perhaps a singular NT throttles the current and then explicitly measured on a seventh-of-a-micron-long section of a 1.4 nm wide armchair tubule. Except for the miniscule size, the setup resembled a field-effect transistor: the current through the tube depends on the bias voltage between the ends and the potential in the middle of the tube (gate). A symmetric and stiff NT allows no defects and almost no phonons at low temperature, with very little scattering and the phase coherent across the entire length. It behaves like "particle-in-a-box" and the box is so small that the electron motion is quantized, so that only a few energy levels are possible. Plus, the capacitance C of this box is so small that adding or removing just one electron is energetically costly, the e^2/C being greater than the thermal energy which results in noticeable Coulomb blockade barrier. Overall it makes the energy levels involved in a conductance event visibly spaced, while the electron can only glide smoothly from source to drain if a nice overall slope is in place. This happens only at a certain gate-voltage, which adjusts the ladder of energy levels up or down and was indeed observed as a sequence of sharp peaks in the current. Similarly, a gradual change in the basis causes a stepwise rather than smooth growth of current, demonstrating again the quantum behavior of a nanotube-wire. To suppress all kinds of thermal perturbation, these studies required very low temperatures, from 10 K down to just millikelvins above absolute zero.

As a molecule, a nanotube is often assumed to be structurally perfect: a cylinder with hexagonal walls terminated by caps with the necessary 12 pentagons. Near the ends, topology related changes in the density of states has been recently investigated experimentally and theoretically [33]. Furthermore, as a tiny material structure grown at highly non-equilibrium conditions, a nanotube may well have some level of quenched disorder. The presence of point defects in a one-dimensional wire can have dramatic effects on its electronics. A special role of pentagon–heptagon (5/7) insertion is due to their ability to change the helical symmetry of a nanotube (see next section) and therefore its band-structure. Two adjacent segments form a hetero-junction and a detailed theoretical analysis of the corresponding density of states has been reported [34, 35]. Such metal/semiconductor or semiconductor/semiconductor junctions could serve as the building blocks for nanoscale electronic devices, a quasi-1D quantum well or (with possible addition of a third terminal) a gated channel. Indeed, an experimentally functioning carbon nanodevice has been reported [36]: a kind of nano-diode with the clear rectification signature is suggested to be due to existence of a 5/7 defect in the nanotube wall. We will see in the next section that such defects also have a profound mechanical meaning and could, in principle, be induced fortuitously or deliberately by mechanical deformation [37, 38]. A design of a "T-junctions" has been proposed [39] as a prototype building block for a 2D network of nanoscale devices [Namely, (5,5)–(10,0)–(5,5) and (9,0)–(10,0)–(9,0) are shown to be stable and to have metal-semiconductor–metal properties.]

4. MECHANICAL BEHAVIOR

Unlike the rigid 3D-lattice of diamond, the 2D-arrangement of atoms in a graphene nanotube wall allows some out-of-plane flexibility. Combined with the strength of constituent bonds, this promises spectacular mechanical properties. Common graphite doesn't strike one as a very strong material. However, the minuscule diameter of nanotubes merely leaves no room for numerous imperfections and microcrevices that make a pencil lead so brittle. As the nanotube studies progressed, several groups reported [40–42] high-resolution images of largely distorted tubes with no traces of fracturing (Fig. 6). However, it was not always clear if this is truly elastic of may be partially due to embedded defects, like pentagonal or heptagonal rings. Atomistic simulations [41] reproduce the bent tube shape very similar to that documented by high resolution TEM. More recent controllable nanotube manipulations [31, 43, 44] with an AFM tip support the notion of their exceptional resilience. In such manipulations the interaction of the tube with the substrate plays an important role in stabilizing the strained configurations and is estimated as 0.8 ± 0.3 eV Å^{-1} for a 10 nm tubule on a hydrogenated Si(1 0 0) surface [31]. Interestingly, on this scale "weak" van der Waals forces produce significant flattening of the cross-section of the tubules [31]: the

Fig. 6. A TEM photograph of a multiwalled carbon tube, bent beyond the buckling point and displaying a distinct kink in the wall [40].

height/diameter of the tube is reduced by 0.3 nm, or almost 0.6 nm at the crossing of two tubules, as Fig. 7 demonstrates.

Calculations show the energy cost of deforming a nanotube [45], which agrees well with elastic parameters known for graphite, or found by first-principle theoretical methods. More surprising was the presence of the "humps and bumps" on the strain energy curves beyond the simple Hooke's law [46]. They indicated some abrupt changes in the molecule under mechanical load and each singularity in the stress-strain curve corresponds to a sudden shape switch of initially perfect cylinder. All generic modes of mechanical load have been studied this way: bending, torsion and axial compression. The nanotube is seen to snap from one shape to the next, emitting visible acoustic waves along its walls at every "crunch". These "crunchy molecules" never actually break, but reversibly accommodate external stress. It became clear that, besides the similarity with the patterns seen in experiment, the observed buckling phenomena resemble the instabilities well known in macroscopic elasticity of hollow shells. In application to nanotubes the correspondence between the elastic shell model and molecular dynamics is remarkable: laws of continuum mechanics are amazingly robust and allow one to treat even intrinsically discrete objects of only few atoms in diameter [46].

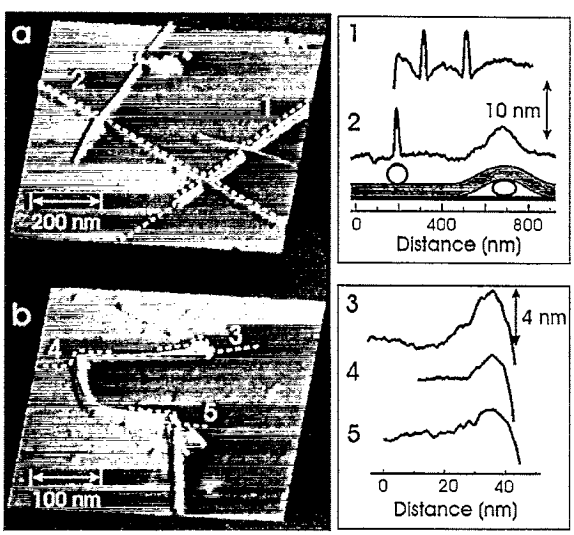

Fig. 7. Non-contact AFM images of elastically deformed CNT on a hydrogenated Si(1 0 0) surface [31]. (a) A height of the nanotube along profile 1 is significantly reduced. (b) Strongly bent nanotube with buckling in heavily strained region. (profiles 3–5).

The ability of a nanotube to sustain axial force to some level, but then to cleverly buckle sideways is quite ingenious for its use as a nanoprobe in a scanning microscope [47]. A nanotube, both stiff and gentle, can be a smart tool, whose gentle touch does not damage the sample and allows the probe itself to "survive the crash" if such happens. At the same time, its slenderness allows one to image sharp topographic details.

A correspondence of atomistic model and macroscopic structural mechanics can be achieved with the proper choice of parameters of the continuum shell [46]. Based on empirical basal in-plane stiffness for graphite and calculated flexural rigidity of a graphene sheet, a choice of the shell parameters is $Y_s = 4$ TPa and effective thickness $h = 0.09$ nm. The small value of the thickness simply reflects the fact that flexing is much easier than stretching for a single graphite sheet, while the large modulus is in fact consistent with the standard value for graphite, if one takes into account the normal spacing, $c = 0.34$ nm, between the sheets in a stack: $Y_d(h/c) = 1$ TPa. The shell model has the benefits of any reductionist approach and allows one to handle larger systems, multiwall tubes or "onions". A hydrostatic compressibility, bending stiffness, or even bending strength of a multiwall tube can be estimated [48].

Calculated bending stiffness appears to be very high for the thinnest single- or double-walled nanotubes and can surpass the commonly expected level by a factor of 2–4, although it converges to normal values for the thicker nanotubes containing many walls. This can serve as a partial explanation of the measured exceptional Young's modulus [48, 49]. In spite of some consonance with the shell model (which agrees in turn with the common graphite data), the extracted highest values, up to 4 TPa, can not be easily explained. Later measurement of the bending stiffness with the AFM tip [43] allows one to estimate the nanotube Young's modulus as 1.3 TPa.

The bending strength of a multiwall tube, measured explicitly in the same controllable experiment [43], provides an interesting example of how efficient the

shell model can be. The value of bending strength is due to the delamination of the layers in the multiwall nanotube, on the compression side. To calculate such bending strength, we can use the shell model and to approximate the delamination event as a buckling of an elastically-supported ($C_{33} > 0$) plate, as described by the fourth-order ODE [48],

$$Y_s I_s u^{IV} + c \cdot \sigma_{compr} u^{II} + (C_{33}/c)u = 0. \quad (3)$$

Here $c = 0.34$ nm, $Y_s h \approx C_{11} \cdot c$, the moment of inertia $I_s = h^3/12$ and u is the deviation of the outmost layer from its normal position at the distance c from the nearest neighbor. The first bifurcation can be found then to occur at $\sigma_{compr} = (h/\sqrt{3}c)\sqrt{C_{11}C_{33}} \approx 29$ GPa. (We use here standard for graphite values $C_{11} \approx 1$ TPa and $C_{33} \approx 36$ GPa, the latter representing the "soft" van der Waals interlayer forces.) This is in excellent agreement with the reported values, 14.2 ± 8.0 GPa, with the greatest detected 28.5 GPa, in spite of possible effects of the overall cylindrical curvature. Bifurcations are notoriously sensitive to the minor influences, which makes – in this case – the large spread of measured values [43] an almost encouraging feature.

How strong in tension is a carbon nanotube? It is too small to be pulled apart with one's hands and too strong for tiny "optical tweezers", for example. The proper instruments are still to be built, or experimentalists should wait until nanotubes grow longer in chemists laboratories. (A strain-tests on nanotubes imbedded in a polymer matrix composite provides a crude estimate of their tensile strength [50].) In the meantime, some tests are being done in computer modeling [38, 46, 51]. In molecular dynamics simulation, the high-strain-rate proceeds in a very peculiar manner. Fast stretching elongates the hexagons in the tube wall, until at the critical point an atomic disorder suddenly nucleates: one or a few C–C bonds break almost simultaneously and the resulting "hole" in a tube wall becomes a crack precursor. The fracture propagates very quickly along the circumference of the tube. A further stage of fracture displays an interesting feature, the formation of two or more distinct chains of atoms, $\cdots$=C=C=C=$\cdots$, spanning the two tube fragments. The vigorous motion (substantially above the thermal level) results in frequent collisions/touching between the chains, which leads to their merging and soon only one of them survives. A further increase of the distance between the tube ends does not break this chain, which elongates by increasing the number of carbon atoms that pop out from both sides into the necklace. This scenario is similar to the monoatomic chain unraveling suggested in field-emission experiments, where the electrostatic force unravels the tube like the sleeve of a sweater. Notably, the breaking strain in such fast-snap simulations is as about 30% and varies with temperature and the strain rate. For a rope of nanotubes this translates in a more than 100 GPa breaking stress.

Fracture, of course, is a kinetic process where time is an important parameter. Even a small applied tension, as any non-hydrostatic stress, makes nanotube metastable and a generation of defects energetically favorable. In order to study a slow strength-determining degradation processes, preceding the fracture, one should either perform extensive simulations at exceedingly elevated temperature [38], or to apply dislocation theory [52]. In a crystal lattice such as the wall of a CNT, a yield to a great tension begins with a homogeneous nucleation of a slip by the shear stress present [Fig. 8(a)]. The non-basal edge dislocations emerging in such slip have a well defined core, a pentagon–heptagon pair, 5/7. Therefore the prime dipole is equivalent to the Stone–Wales (SW) defect [3], Fig. 8(b). It can be shown [37] that the energetics of such nucleation and of the glide of a single 5/7 dislocation, explicitly depend on nanotube helicity, e.g.

$$E_{glide} = 64 \cdot \sin(2\chi + \pi/3) \cdot \epsilon, eV \quad (4)$$

per one step $b = 0.246$ nm. The energy gained in nucleation has another dependence on helicity, $\sim\sin(2\chi + \pi/6) \cdot \epsilon$: the SW rotation gains more energy

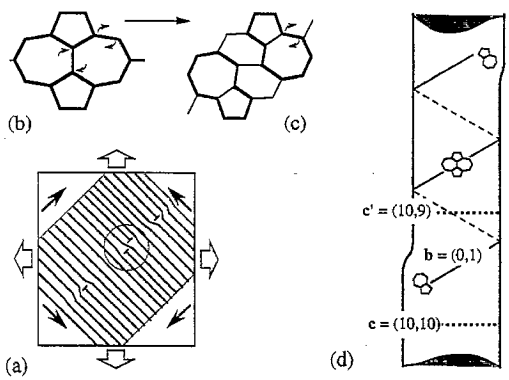

Fig. 8. (a) Under tension, the shear components cause a glide of existing dislocations or a formation of new dislocation dipole (circled) in a perfect material. (b) In an armchair CNT, the first Stone-Wales rotation of an equatorially oriented bond into a vertical position creates a nucleus of relaxation. (c) SW-rotations marked by arrows show further evolution as a couple of dislocations guided away from each other. (d) The change of the CNT chirality and a stepwise change of diameter causes the corresponding variations of electrical properties. Formation of a next SW defect continues the necking process, unless the dislocations pile-up at insufficient temperature (adapted from [37]).

in the armchair ($\chi = \pi/6$) tube, making it the weakest or the most inclined to nucleation of the dislocations, in contrast to the zigzag ($\chi = 0$) where the nucleation is least favorable. Further evolution of the emerging dipole can lead to either brittle cleavage or, at very high temperatures, plastic flow: a glide of dislocations away from each other, Fig. 8(c). Under high stress, the dislocations depart from each other along helical paths, leaving behind a nanotube of smaller diameter, well defined new symmetry and changed electrical properties. Atomistics of this glide represents a further sequence of SW rotations of a certain type. Using the same basis in hexagonal lattice used for the helicity indexes, every 5/7 core can be assigned a proper Burgers vector **b**. Then the change of helicity due to the presence of a defect is described by equation [37],

$$(c'_1, c'_2) = (c_1, c_2) - (b_1, b_2), \tag{5}$$

with the corresponding reduction of diameter. While the dislocations of the first dipole glide away, another generated dipole can result in further narrowing and elongation under stress, thus forming a neck. The progression of helicities, following the schematics in Fig. 3 will be [37]: $(10,10) \rightarrow (10,9) \rightarrow (10,8) \rightarrow \cdots (10,0) \rightarrow [(9,1)$ or $(10,1)] \rightarrow (9,0) \rightarrow [(8,1)$ or $(9,-1)] \rightarrow (8,0) \rightarrow [7,1)$ or $(8,-1)] \rightarrow (7,0)$ etc. Correspondingly, the diameter changes stepwise, $d = 1.36$, 1.29, 1.22, 1.16 nm, etc. The local stress grows in proportion and this "quantized" necking can be terminated by a cleave at late stages, as occurs for macroscopic material. Interestingly, such plastic flow is accompanied by a change of electronic structure of the emerging domains, governed by the vector (c_1,c_2), as discussed in the previous section. This resembles the coupling of mechanical and transport properties in nanowires [53] and suggests in principle the possibility of tuning the properties of nanotubes or their junctions.

An accurate computer simulation [38] demonstrate clearly the sequence of SW-rotations and the emerging topological defects. It provides important absolute values for the energetics of the relaxation process: the defect formation energy, activation barriers and their stress dependence. The activations energies are high and the kinetic rate is often negligible. For example, the barrier [38] $E^* \approx (6 - 20 \cdot \epsilon)$ eV for the Stone–Wales bond rotation even at $\epsilon = 20\%$ strain is about 2 eV high (this barrier apparently corresponds to the lower of the possible channels identified in [54]). At room temperature, this means many years expectation time for a single bond rotation (dislocation slip) in a nanotube even a meter long. Of course, pre-existing defects, radiation, or the presence of aggressive chemicals will have deteriorating effect on the strength.

5. APPLICATIONS FOR THE FUTURE

Potential applications of fullerene nanotubes abound and offer a diversified portfolio attractive to even a cautious technology investor. One first group includes macro-applications, where the nanotubes line up to form a light strong wire or a composite. These applications require a real volume production of the critical components, nanotubes of greater length that are free of defects. The hollow structure of nanotubes, their ability to collapse under compression and then to restore the volume [55], is good for shock-absorbing materials. Outstanding thermal conductivity along the tubes-filaments, combined with relatively little heat transport in the perpendicular direction, can be of interest for microelectronics, where progressing miniaturization demands better heat-sinks.

Down in scale is an even broader spectrum of things where CNT are used on an individual basis and these make a second group of applications, a significant insertion in the nanotechnology. Already demonstrated crash-proof nanoprobes for scanning microscopy exploit the mechanical resilience and conductivity of CNT. A stiff and light CNT properly attached/suspended at both ends can serve as a high frequency mechanical resonator, like those successfully made out of Si by a dry etch technique [56, 57]. Open-end "nanostraws" can penetrate into a cellular structure for chemical probing, or be used as nano-pipettes to inject molecules into living cells with almost no damage to the latter. CNT with a wide range of electrical properties will serve in smaller and faster computing machines of the future. A pure-carbon metal–semiconductor heterojunction has been recently analyzed (see Section 3). At low temperatures, quantum transport renders NT genuine quantum wires, a core of a "single-electron transistor". A controllable cutting by an STM tip to a desired length allows to change the electronic properties [58]. Modification of the density of states induced by stress and therefore coupling of the external mechanical stimuli with the conductance places CNT into the family of future sub-microelectro-mechanical systems, MEMS. Indeed, with the recently reported C_{60}-based electromechanical amplifier [59], one can anticipate even better performance from a nanotube, since it is prone to mechanical distortions. Sharp conducting NT-tips could serve as electron guns, lighting up the phosphor layer on flat-panel displays. All these applications pose a common problem: how to properly implant the CNT with desirable properties into a larger device or a circuit. Beyond that, to become truly practical, this has to be done multiply and reproducibly. The issues of multiplicity and batch fabrication enter the agenda as soon as the feasibility is demonstrated.

REFERENCES

1. Kroto, H.W., Heath, J.R., O'Brien, S.C., Curl, R.F. and Smalley, R.E., *Nature*, **318,** 1985, 162.
2. Kratschmer, W., Lamb, L.D., Fostiropoulos, K. and Huffman, D.R., *Nature*, **347,** 1990, 354.
3. Dresselhaus, M.S., Dresselhaus, G. and Eklund, P.C., *Science of Fullerenes and Carbon Nanotubes*. Academic Press, San Diego, 1996.
4. Ebbesen, T.W., Editor., Carbon Natnotubes: Preparation and Properties. CRC Press, Tokyo, 1997.
5. Iijima, S., *Nature*, **354,** 1991, 56.
6. Sattler, K., *Carbon*, **33,** 1995, 915.
7. Krishnan, A. *et al.*, *Nature*, **388,** 1997, 451.
8. Zhang, Q., Yi, J.-Y. and Bernholc, J., *Phys. Rev. Lett.*, **66,** 1991, 2633.
9. Thess, A. *et al.*, *Science*, **273,** 1996, 483.
10. Haufler, R.E. *et al.*, *J. Phys. Chem.*, **94,** 1990, 8634.
11. Colbert, D.T. *et al.*, *Science*, **266,** 1994, 1218.
12. Ebbesen, T.W. and Ajayan, P.M., *Nature*, **358,** 1992, 220.
13. Bethune, D.S. *et al.*, *Nature*, **363,** 1993, 605.
14. Iijima, S. and Ichihashi, T., *Nature*, **361,** 1993, 603.
15. Mintmire, J.W., Dunlap, B.I. and White, C.T., *Phys. Rev. Lett.*, **68,** 1992, 631.
16. Hamada, N., Sawada, S. and Oshiyama, A., *Phys. Rev. Lett.*, **68,** 1992, 1579.
17. Saito, R., Fujita, M., Dresselhaus, G. and Dresselhaus, M.S., *Appl. Phys. Lett.*, **60,** 1992, 2204.
18. Kane, C.L. and Mele, E.J., *Phys. Rev. Lett.*, **78,** 1997, 1932.
19. Mintmire, J.W., Robertson, D.H. and White, C.T., *J. Phys. Chem. Solids*, **54,** 1993, 1835.
20. Saito, R., Dresselhaus, G. and Dresselhaus, M.S., *J. Appl. Phys.*, **73,** 1993, 494.
21. Ebbesen, T.W. *et al.*, *Nature*, **382,** 1996, 54.
22. Fischer, J.E. *et al.*, *Phys. Rev.*, **B55,** 1997.
23. Bockrath, M. *et al.*, *Science*, **275,** 1997, 1922.
24. Dai, H., Wong, E.W. and Lieber, C.M., *Science*, **272,** 1996, 523.
25. Tans, S.J. *et al.*, *Nature*, **386,** 1997, 474.
26. Wildoer, J.W.G., Venema, L.C., Rinzler, A.G., Smalley, R.E. and Dekker, C., *Nature*, **391,** 1998, 59.
27. Odom, T.W., Huang, J.-L., Kim, P. and Lieber, C.M., *Nature*, **391,** 1998, 62.
28. Dresselhaus, M.S., *Nature*, **391,** 1998, 19.
29. Louie, S., private communication.
30. Ruoff, R.S., Tersoff, J., Lorents, D.C., Subramoney, S. and Chan, B., *Nature*, **364,** 1993, 514.
31. Hertel, T., Martel, R. and Avouris, P., *J. Phys. Chem.*, **B102,** 1998, 910.
32. Langer, L. *et al.*, *Phys. Rev. Lett.*, **76,** 1996, 479.
33. Carroll, D.L. *et al.*, *Phys. Rev. Lett.*, **78,** 1997, 2811.
34. Charlier, J.-C., Ebbesen, T.W. and Lambin, P., *Phys. Rev.*, **B53,** 1996, 11108.
35. Chico, L., Crespi, V.H., Benedict, L.X., Loui, S.G. and Cohen, M.L., *Phys. Rev. Lett.*, **76,** 1996, 971.
36. Collins, P.G., Zettl, A., Bando, H., Tehss, A. and Smalley, R.E., *Science*, **278,** 1997, 100.
37. Yakobson, B.I., *Appl. Phys. Lett.*, **72,** 1998, 918.
38. Buongiorno Nardelli, M., Yakobson, B.I. and Bernholc, J., *Phys. Rev.*, **B57,** 1998, R4277.
39. Menon, M. and Srivastava, D., *Phys. Rev. Lett.*, **79,** 1997, 4453.
40. Despres, J.F., Daguerre, E. and Lafdi, K., *Carbon*, **33,** 1995, 87.
41. Iijima, S., Brabec, C.J., Maiti, A. and Bernholc, J., *J. Chem. Phys.*, **104,** 1996, 2089.
42. Chopra, N.G. *et al.*, *Nature*, **377,** 1995, 135.
43. Wong, E.W., Sheehan, P.E. and Lieber, C.M., *Science*, **277,** 1997, 1971.
44. Falvo, M.R. *et al.*, *Nature*, **389,** 1997, 582.
45. Robertson, D.H., Brenner, D.W. and Mintmire, D.W., *Phys. Rev.*, **B45,** 1992, 12592.
46. Yakobson, B.I., Brabec, C.J. and Bernholc, J., *Phys. Rev. Lett.*, **76,** 1996, 2511.
47. Dai, H., Hafner, J.H., Rinzler, A.G., Colbert, D.T. and Smalley, R.E., *Nature*, **384,** 1996, 147.
48. Yakobson, B.I., to be published.
49. Treacy, M.M.J. and Ebbesen, T.W., *Nature*, **381,** 1996, 678.
50. Wagner, H.D., Lourie, O., Feldman, Y. and Tenne, R., *Appl. Phys. Lett.*, **72,** 1998, 188.
51. Yakobson, B.I., Campbell, M.P., Brabec, C.J. and Bernholc, J., *Computational Mater. Sci.*, **8,** 1997, 341.
52. Yakobson, B.I., Dynamic Topology and Yield Strength of Carbon Nanotubes (Edited by R.S. Ruoff, K.M. Kadish), vol. 5, p. 549. Fullerenes – Electrochemical Society, ECS, Pennington, 1997.
53. Landman, U., Luedtke, W.D., Salisbury, B.E. and Whetten, R.L., *Phys. Rev. Lett.*, **77,** 1996, 1362.
54. Scuseria, G.E., *Science*, **271,** 1996, 942.
55. Fischer, J.E., private communication.
56. Cleland, A.N. and Roukes, M.L., *Appl. Phys. Lett.*, **69,** 1996, 2653.
57. Cleland, A.N. and Roukes, M.L., *Nature*, **392,** 1998, 160.
58. Venema, L.C. *et al.*, *Appl. Phys. Lett.*, **71,** 1997, 2629.
59. Joachim, C. and Gimzewski, J.K., *Chem. Phys. Lett.*, **265,** 1997, 353.